

This is a pre-print of a revised manuscript re-submitted to Paleoceanography and Paleoclimatology and posted to EarthArXiv. It has not yet finished peer review and will likely change before it is finalized. Comments are very welcome, and should be sent to the corresponding author (cmlowery@utexas.edu)

Elevated Post K-Pg Export Productivity in the Gulf of Mexico and Caribbean

Christopher M. Lowery^{1*}, Timothy J. Bralower²

¹University of Texas Institute for Geophysics, Austin, TX

²Pennsylvania State University, University Park, PA

*corresponding author: cmlowery@utexas.edu

Abstract

The global heterogeneity in export productivity after the Cretaceous-Paleogene (K-Pg) mass extinction is well documented, with some sites showing no change on geologic timescales, some demonstrating sustained decline, and a few showing a somewhat surprising increase. However, observational data come from sites so widespread that a key outstanding question is the geographic scale of changes in export productivity, and whether similar environments (e.g., open ocean gyres) responded similarly or whether heterogeneity is unrelated to environment. To address this, we developed three new Ba/Ti export productivity records from sites in the Gulf of Mexico and Caribbean which, combined with published data from a fourth site in the Chicxulub Crater itself, allows us to reconstruct regional changes in post K-Pg export productivity for the first time. We find that, on a regional scale, export productivity change is homogenous, with all four sites showing a ~300 kyr period of elevated export production just after the boundary, followed by a longer period of decline. Interestingly, this interval of elevated export production appears to coincide with the post K-Pg global micrite layer, which is thought to at least partially have been produced by blooms of carbonate-producing cyanobacteria and other picophytoplankton. We note from a global comparison of sites that elevated export productivity appears to be most common in oligotrophic gyres, which suggests that changing plankton ecology evidenced by

23 the micrite layer altered the biological pump, leading to a temporary increase in export production in
24 these settings.

25 **Plain Language Summary**

26 Primary producers are the base of the food chain; this group was severely damaged by the
27 environmental effects associated with the Cretaceous-Paleogene mass extinction. Determining how
28 primary production recovered after this calamity is an important foundation for understanding how
29 ecosystems recovered. Most previous work on this topic has focused on a process called export
30 production, whereby organic carbon produced by phytoplankton is transferred to the ocean interior (some
31 of which sinks to the seafloor and is buried). This work has shown that although most parts of the ocean
32 recorded a decline in export production after the extinction event, some regions actually showed an
33 increase. However, it was not clear on what geographic scale these differences occurred, or what caused
34 them. We generated three new records of export production from a single region, the Gulf of
35 Mexico/Caribbean Sea, and found a consistent increase in export production at each site for the same
36 period of time after the extinction event. Comparison with other sites with increased export production
37 shows that many are from open ocean gyres and suggests that these regions were predisposed to increased
38 export production in the earliest Paleocene because they were characterized by low productivity prior to
39 the extinction.

40 **1. Introduction**

41 The end Cretaceous mass extinction is associated with a severe disruption of marine productivity
42 (Hsü and Mackenzie, 1985; Zachos et al., 1989; D'Hondt et al., 1998; Coxall et al., 2003; Birch et al.,
43 2016). A reduction in sunlight caused by dust, soot, and sulfate aerosols ejected by the Chicxulub impact
44 resulted in a reduction in photosynthesis which is believed to have led to the collapse of marine food webs
45 (Alvarez et al., 1980; D'Hondt et al 1998). Models show that the reduction in insolation lasted only a few
46 years after the impact (Toon et al., 1997; Bardeen et al., 2016; Brugger et al., 2016; Artemieva et al.,

47 2016; Artemieva and Morgan, 2020), removing the proximal external stress on marine primary producers
48 and clearing the way for the recovery of primary production. How, exactly, marine productivity recovered
49 has been a central focus of K-Pg boundary research for decades; the K-Pg mass extinction represents a
50 geologically unique disruption of marine ecosystems, perhaps the only major event in Earth history which
51 happened faster than modern climate change and environmental disruption. Modern oceans are likely on
52 the verge of a major reorganization of dominant plankton types due to warming, acidification, and
53 changes in circulation patterns (e.g., Barton et al., 2016; Jonkers et al., 2019), and primary production is
54 expected to decline 20% due to warming (Moore et al., 2018). The earliest Paleocene provides a window
55 into understanding how such ecological changes may impact food webs and marine carbon burial.

56 Of course, we can't observe ancient primary production in the euphotic zone directly, and so most
57 work on the collapse and recovery of productivity after the K-Pg boundary is focused on sedimentary
58 records of export production (the transfer of particulate organic matter from the euphotic zone to the deep
59 sea; e.g., Passow and Carlson, 2012)). The movement of particulate organic matter (POM) from the
60 euphotic zone to the seafloor is complicated and can be divided into a series of steps, all of which are
61 influenced by different processes. Most net primary production (NPP) occurs in the euphotic zone
62 (dependent on sunlight penetration but typically defined as 0-100 or 200 m water depth; Passow and
63 Carlson, 2012), and the large majority of POM is remineralized in these near surface waters. The precise
64 amount varies by region and season, but typically ~ 90% of NPP is consumed and recycled before it can
65 sink out of the euphotic zone. The movement of POM out of the euphotic zone is typically what
66 biological oceanographers define as "export flux" or "export productivity" (Passow and Carlson, 2012).
67 Paleoceanographers typically use the latter term to refer to the whole process by which POM is buried in
68 the sediments. However, here we follow the biological oceanographers and use "export productivity" to
69 refer to this initial sinking out of surface waters, mainly because this is the process that can be tracked in
70 ancient sediments by biogenic barium – see below). As POM continues sinking through the mesopelagic
71 zone (typically defined as 100-1000 m water depth; Passow and Carlson, 2012) it is subject to grazing by

72 mesopelagic organisms of all sizes, which gradually break down long chain organic carbon molecules
73 back to their constituent inorganic carbon molecules, turning POM into dissolved organic carbon (DOC)
74 and then dissolved inorganic carbon (DIC) (e.g., Boyd and Trull, 2007). The amount of remineralization
75 that occurs in the mesopelagic zone is controlled by the rate at which the POM is sinking (i.e., how long it
76 is exposed to mesopelagic grazers), the composition of the grazing ecosystem, and the quality of the
77 organic carbon (i.e., is it labile and easy to degrade or refractory and more difficult to break down) (e.g.,
78 Buessler and Boyd, 2009; Henson et al., 2012). POM which sinks below the mesopelagic zone is
79 effectively removed from the short-term carbon cycle, and so the export of organic matter below 1000 m
80 is often referred to as “sequestration flux” (e.g., Passow and Carlson, 2012) or “transfer efficiency”
81 (Henson et al., 2012). By this point, most remineralization has occurred, but POM sinking out of the
82 mesopelagic zone has traveled through less than one third of the average depth of the ocean, and
83 additional remineralization occurs all the way to (and at) the seafloor, before surviving POM is buried and
84 removed from the carbon cycle on geologic time scales (referred to as “burial flux” by Griffith et al.,
85 2021). The amount of net primary production that reaches the deep sea varies by region and is largely
86 controlled by plankton ecology (Henson et al., 2012), but on the whole only 1-3% of modern net primary
87 production reaches the deep ocean or sediments (e.g., Müller and Suess, 1979; de la Rocha and Passow,
88 2007; Griffith et al., 2021).

89 Initial reconstructions of productivity change across the K-Pg boundary focused on carbonate
90 proxies, specifically carbonate mass accumulation rates and carbon stable isotopes (e.g., Hsü and
91 Mackenzie, 1985; Zachos et al., 1989). A drop in carbonate mass accumulation rate in the deep sea has
92 been observed at many boundary sites across the globe, and is interpreted to represent a reduction in the
93 production of carbonate by pelagic calcifiers like calcareous nannoplankton and planktic foraminifera
94 (e.g., D’Hondt et al., 1998), both of which suffered a severe (>90% species diversity) extinction at the K-
95 Pg boundary (e.g., Thierstein, 1982; Bown, 2005; Fraass et al., 2015; Lowery et al., 2020). The most
96 striking carbonate proxy response, though, is the collapse of the $\delta^{13}\text{C}$ gradient between the surface ocean

97 and the deep sea (Zachos and Arthur, 1986; Zachos et al., 1989; D'Hondt et al., 1998; Coxall et al., 2003;
98 Alegret et al., 2012; Esmeray-Senlet, 2015; Birch et al., 2016). In the modern ocean (and likely since
99 phytoplankton first evolved) the sinking of ^{12}C -rich organic matter depletes the surface ocean and
100 enriches the seafloor in that light isotope, resulting in an isotopic gradient from surface to seafloor. This
101 gradient collapsed at the Cretaceous-Paleogene (K-Pg) boundary (e.g., Kump, 1991), reflecting a
102 reduction in export production and a weakening of the biological pump for 1.8 myr (Birch et al., 2016,
103 2021). Taking into account observed changes in planktic foraminifer ecology and physiology (which
104 account for a portion of the change in the $\delta^{13}\text{C}$ gradient – Birch et al., 2016, 2021), modelling suggests
105 that a ~50% decrease in the amount of organic carbon exported from the euphotic zone, from 10% of net
106 primary production to 5%, would account for the observed collapse of the $\delta^{13}\text{C}$ gradient (D'Hondt et al.,
107 1998; Henehan et al., 2019).

108 The continued flux of some organic matter to the deep ocean is confirmed by fossil data which
109 indicate a lack of extinction in some groups of pelagic fishes (Doyle, 1979; Siebert and Norris, 2015) and
110 deep sea benthic foraminifera (e.g., Culver, 2003; Alegret and Thomas, 2005, 2007, 2009; Alegret et al.,
111 2012, 2021). Meanwhile, geochemical data indicate a rapid recovery of primary producers (Sepúlveda et
112 al., 2009, 2019). One of the most striking features of the benthic foraminiferal record at the K-Pg
113 boundary is how it varies globally. Although no major extinction occurred, assemblage compositions
114 shifted at many sites (e.g., Culver et al., 2003; Alegret et al., 2012, 2021). At some localities, benthic
115 foraminifer assemblages indicate a reduction in the flux of organic matter to the seafloor, but others show
116 no change across the boundary, and some actually indicate an *increase* in organic matter flux (e.g.,
117 Alegret and Thomas 2005, 2007, 2009; Alegret et al., 2012, 2021).

118 In practice, it is difficult to use carbon isotope gradients to reconstruct post K-Pg export
119 production in any sort of geographic detail. Isotopic analysis of planktic and benthic foraminifera requires
120 well-preserved carbonate material, otherwise diagenetic overprinting will obscure the signal. Localities
121 with well-preserved 66-myr-old foraminifera are not particularly common, and for that reason carbon

122 isotope gradients have only been produced from a handful of well-studied sites like Walvis Ridge (Hsu
123 and Mackenzie, 1985; D'Hondt, 1998a; Coxall et al., 2006; Birch et al., 2016, 2021), Shatsky Rise
124 (Zachos and Arthur, 1986; Zachos et al., 1989; Coxall et al., 2006), J-Anomaly Ridge (Zachos and
125 Arthur, 1986), and São Paulo Plateau (Zachos and Arthur, 1986). While these sites have all yielded high
126 quality data that have fundamentally changed our understanding of K-Pg recovery, they only cover a
127 small part of the ocean.

128 For this reason, additional proxies not dependent on pristine microfossil preservation are
129 necessary. Benthic foraminifera, which track burial flux of POM, are one such proxy, and another is
130 based on barium. Biogenic barium abundance in marine sediments (where it is commonly preserved as
131 barite – BaSO₄) has been shown to correlate with export production in the modern and ancient ocean
132 (Dymond et al., 1992; Francois et al., 1995; Eagle et al., 2003; Paytan and Griffith, 2007) and is not
133 subject to the same diagenetic effects as carbon isotopes. Like so many other proxies, though, studies
134 have shown that the relationship between the measurement (biogenic barium) and the thing for which it is
135 a proxy (export production) is not quite as straight forward as it seemed at first. A good recent review of
136 the various processes which can affect the formation, burial, and preservation of marine barite can be
137 found in Carter et al. (2020). Here we summarize the most important processes that impact the
138 reconstruction of changes in export production across the K/Pg boundary.

139 Although marine barite is linked to export production, Ba can also be sourced from detrital
140 settings, and the Ba content can vary from source area to source area (e.g., Carter et al., 2020), so
141 elemental Ba data need to be normalized against a terrigenous element like titanium or aluminum to
142 control for any possible detrital barium component (e.g., Dymond et al., 1992; Payton et al., 1996; Bains
143 et al., 2000; Paytan and Griffith, 2007; Griffith and Paytan, 2012). Most marine barite formation occurs
144 between 200-600 m water depth, where most organic matter remineralization occurs (Martinez Ruiz et al.,
145 2020; Carter et al., 2020), and so biogenic Ba production tracks “export flux” or the amount of POM
146 which sinks below the euphotic zone (see above). However, Ba formation is probably mediated by

147 bacteria which consume oxygen during remineralization of POM, which means that increased bacteria
148 production could lead to increased barite formation (e.g., Dehairs et al., 2008; Jacquet et al., 2011;
149 Planchon et al., 2013) without a change in export production. This microbial activity can be influenced by
150 organic matter quality, temperature (as warmer temperatures result in increased bacterial activity), and the
151 composition of the microbial ecosystem itself (Carter et al., 2020). Ba *production* is thus (mostly)
152 correlated directly to the export flux of POM, but the ocean is undersaturated in barite, which means that
153 70% of particulate barite (and more in anoxic regions) dissolves in the water column and the upper few
154 cm of the sediments before it is buried (Carter et al., 2020). This means that the replacement of one
155 watermass with another of a different Ba²⁺ saturation state could lead to a change in barite accumulation
156 which could be misinterpreted as a change in export flux (e.g., Carter et al., 2020).

157 These caveats make it difficult to directly extrapolate from Ba flux to absolute values of export
158 flux in mass of organic carbon per unit time, particularly all the way back in the Paleocene, but if major
159 variables (terrigenous flux, water mass changes) are controlled for then marine barite can provide
160 important insights to changes in export flux. Hull and Norris (2011) used XRF-derived Ba/Ti and Ba/Fe
161 ratios from five K-Pg boundary sites to bolster the export productivity record of benthic foraminifera, and
162 demonstrated that changes in export production across the boundary were indeed geographically
163 heterogeneous, with some sites showing an increase in export production after the boundary.

164 Understanding geographic heterogeneity in export production is necessary to understand the
165 overall recovery of marine primary producers after the K-Pg boundary. In particular, the calcareous
166 nannoplankton, which have the best fossil record among primary producers in the early Paleocene, exhibit
167 geographic heterogeneity in their post K-Pg recovery (Jiang et al., 2010; Schueth et al. 2015; Jones et al.,
168 2019). Post-extinction calcareous nannoplankton assemblages are characterized by a dominance of
169 “disaster taxa,” chiefly *Braarudosphaera* and *Cervisiella*, which eventually give way to a succession of
170 acme events as new Paleocene genera appear and briefly dominate the assemblage (Bown, 2005; Jones et
171 al., 2019; Gibbs et al., 2020). Gibbs et al. (2020) found that some of the survivors and earliest new genera

172 have adaptations which indicate a mixotrophic lifestyle (i.e., they supplemented photosynthesis by
173 ingesting small prey like bacteria); later incoming taxa lack these adaptations, indicating changing trophic
174 conditions (specifically the under exploitation of small prey species following the extinction of many
175 heterotrophic plankton) may have played a role in nanoplankton recovery (Gibbs et al., 2020). The
176 timing of these acme events is geographically variable, and at sites with elevated export productivity after
177 the K-Pg (Shatsky Rise and Chicxulub Crater), it is coincident with an observed decline in export
178 production (Jones et al., 2019). In the ocean today, eutrophic waters tend to be dominated by a few taxa
179 best suited to take advantage of widely available food, while oligotrophic waters tend to have much
180 higher diversity with greater degrees of specialization (e.g., Hallock, 1987). Jones et al. (2019)
181 hypothesized that the recovery of primary producer assemblages (and by extension the ecosystems which
182 they supported) after the K-Pg is similarly linked to nutrient state controlled by the recovery of the
183 biological pump, but the linkages are not well understood and a better picture of export productivity
184 trends is a necessary first step.

185 Unfortunately, the geographic trends in early Paleocene export productivity are still poorly
186 known. Modelling work by Henehan et al. (2019) indicated that typically oligotrophic gyre environments
187 in the North and South Pacific Oceans, the Arctic Ocean, and northern Indian Ocean, would have
188 experienced increased export productivity in a scenario in which global average export productivity
189 declined 50% (in line with estimates of post-K-Pg declines in export production; D'Hondt et al., 1998;
190 Henehan et al., 2019). However, these modelling results are currently unconstrained by data, and sites
191 with observed increases in post-extinction export production (e.g., Shatsky Rise Site 1209; Hull and
192 Norris, 2011) are close to but fall outside of modelled areas of increased post-extinction export
193 production. Although the work of Hull and Norris (2011) represents a significant improvement in
194 observations of export productivity trends, they are still limited to the ocean basin scale: Shatsky Rise in
195 the North Pacific compared to São Paulo Plateau in the South Atlantic compared to Maud Rise in the
196 Southern Ocean. This is a good starting place but leaves open the question of the scale of heterogeneity.

197 Do regions exhibit similar trends (implying an oceanographic driver of variability) or do sites vary even
 198 within a region (implying that variability is driven by local effects or is just stochastic)? To address this
 199 question, we developed three new Ba/Ti datasets from the Gulf of Mexico and Caribbean at Deep Sea
 200 Drilling Project (DSDP) Site 95 and Ocean Drilling Program (ODP) Sites 999 and 1001, which we
 201 combined with published data from International Ocean Discovery Program (IODP) Site M0077 in the
 202 Chicxulub Crater (Lowery et al., 2021) to produce the first regional-scale study (~1700 km) of export
 203 productivity after the K-Pg. This region was modelled to have been characterized by low export
 204 production in the latest Cretaceous (Henehan et al., 2019) and thus may be predicted to exhibit increased
 205 export production after the boundary. We found that earliest Danian export productivity is elevated at all
 206 Gulf of Mexico and Caribbean sites and that an initial reduction in export production occurs ~ 300 kyr

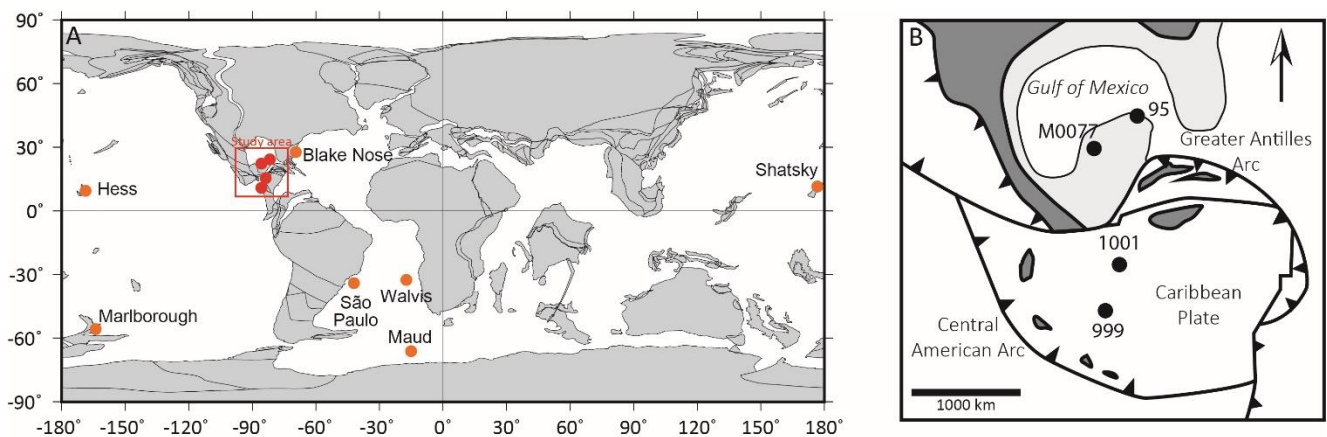


Figure 1. A) Global plate tectonic reconstruction from 66 Ma showing location of our study area (in red) and other notable sites discussed in this paper (in orange). Grey areas are continental blocks, terranes, and plateaus; map from ODSN generated at <https://www.odsn.de/odsn/services/paleomap/paleomap.html>. B) Regional map showing position of our study sites around the time of the K-Pg Boundary. Map modified after Pindell and Barrett (1990) and Snedden et al. (2021). Black indicates land and grey indicates continental platforms.

207 after the boundary at all sites, indicating that export productivity trends are homogeneous at a regional
 208 scale.

209 1.1 Study Sites

210 We looked at three scientific ocean drilling sites in the greater Caribbean region with an
 211 identified and well-preserved K-Pg boundary interval and compared them to published XRF data from
 212 IODP Site M0077 in the Chicxulub Crater (Figure 1). An additional site, DSDP Site 536, below the

213 Campeche Escarpment in the southeastern Gulf of Mexico (Buffler et al., 1984), was considered but
214 rejected because a preliminary examination of planktic foraminifera in the nominally lowermost
215 Paleocene cores found a mix of biozones ranging from the Cretaceous to the late Paleocene, indicating
216 significant reworking and/or drilling disturbance, suggesting that XRF data would be untrustworthy. All
217 four of these sites appear to have been at roughly bathyal water depths in the earliest Danian (Worzel et
218 al., 1983; Buffler et al., 1984; Sigurdsson et al., 1997; Lowery et al., 2018). These tropical/subtropical
219 sites are characterized by pelagic carbonate deposition throughout the study interval.

220 DSDP Site 95, drilled in 1970 on the northeasterly margin of the Yucatan Platform on the
221 Campeche Escarpment (Worzel et al., 1973), contains the correct order of planktic foraminifer biozones
222 and decent preservation in a mostly-complete section overlying the K-Pg impact layer. The Chicxulub
223 impact (and associated earthquakes, tsunamis, and seiche waves) caused widespread mass-wasting across
224 the Gulf of Mexico, resulting in K-Pg boundary deposits 10s to 100s of m thick (e.g., Bralower et al.,
225 1998; Denne et al., 2013; Sanford et al., 2016). Site 95, due to its perched position on the edge of the
226 Yucatan Platform, only has ~ 3 m of reworked Cretaceous material and impact debris (Figure 2A). The
227 top of the K-Pg boundary layer occurs at the top of Core 13. This is not the K-Pg boundary per se,
228 because the base of the Paleocene is defined at its Global Stratotype Section and Point at El Kef, Tunisia,
229 as the lowest occurrence of impact material which means that the Cretaceous ended at “the moment of the
230 meteorite impact” (Molina et al., 2009). The impact layer in the Gulf of Mexico is thus technically earliest
231 Danian in age.

232 Site 1001 was drilled in 1995-6 during ODP Leg 165, and is located on a feature called the Hess
 233 Escarpment on the Nicaragua Rise (Figure 1). Shipboard biostratigraphy placed the K-Pg boundary
 234 between Core 1001A-38R-CC and 1001A-39R-1 (Figure 2B). Unlike the thick K-Pg boundary deposits
 235 found in the Gulf of Mexico, here the whole interval is just a few cm thick. Maastrichtian limestone is
 236 overlain by a 1 cm thick dark greenish gray clay, which is in turn overlain by a 3.5 cm bluish gray
 237 claystone containing 1 mm scale dark green spheroids interpreted to be tektites (Sigurdsson et al., 1997).

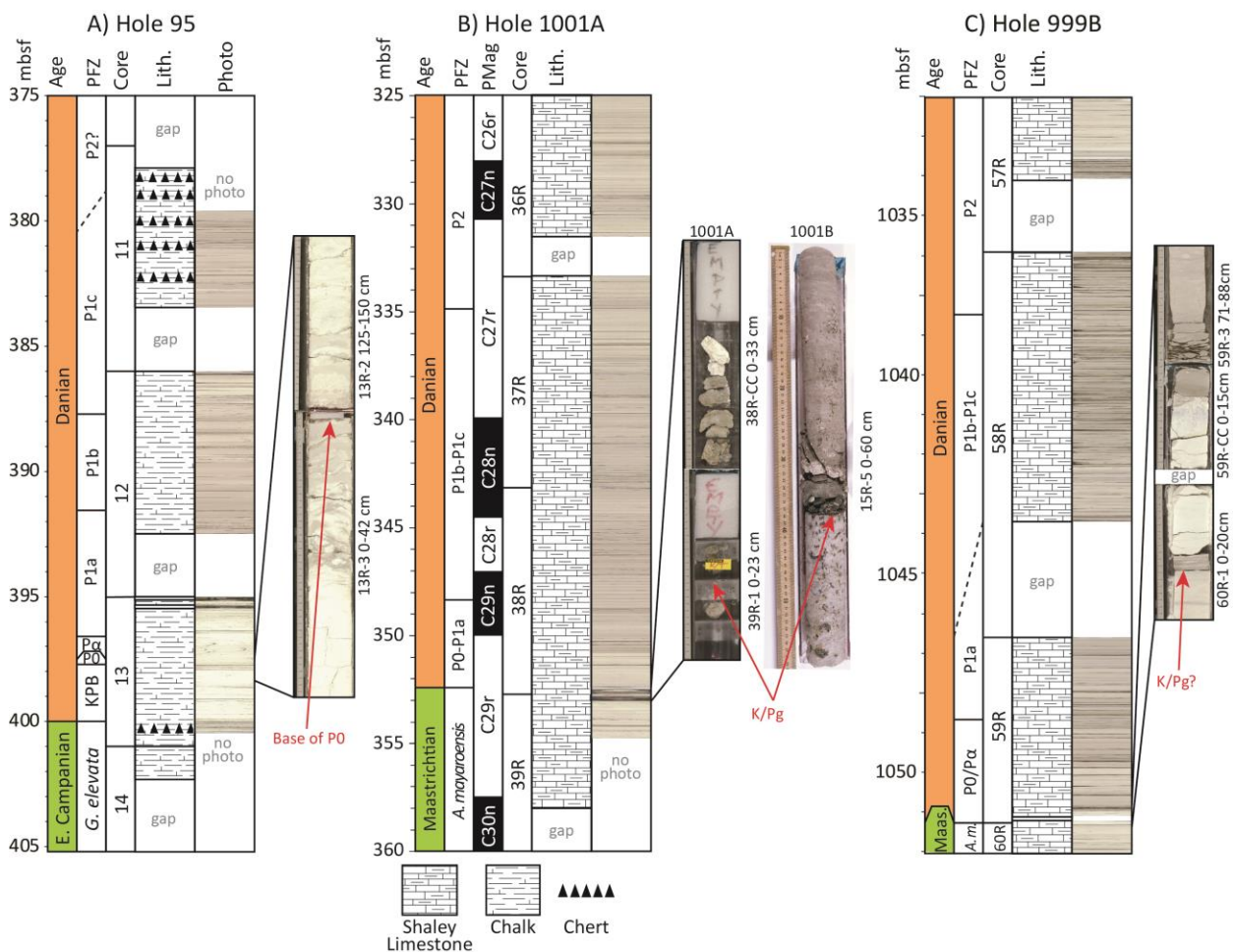


Figure 2. Stratigraphic sections showing lithostratigraphy, core scan photographs, and images of the K-Pg boundary of the studied intervals from DSDP Hole 95, ODP Hole 1001A, and ODP Hole 999B. Lithostratigraphy follows shipboard descriptions Worzel, Bryant et al. (1973) for Site 95 and Sigurdsson et al., 1997 for Sites 999 and 1001). Core scan photographs were collected at the GCR at the same time XRF data were collected (except for the photograph of the K-Pg boundary in Hole 1001B, which is from the ODP photo archives). Mbsf = meters below sea floor, PFZ = Planktic Foraminifer Zone, Lith. = lithology, PMag = Paleomagnetic polarity, E. Campanian = Early Campanian, Maas. = Maastrichtian, G. elevata = Globotruncanita elevata, A.m. and A. mayaroensis = Abathomphalus mayaroensis.

238 This tektite layer is overlain by a 3.5 cm medium gray to greenish gray claystone which contains
239 shocked quartz (Sigurdsson et al., 1997). The boundary sequence is overlain by a 4 cm thick light grey
240 limestone assigned to planktic foraminifer Biozones P0/P α undifferentiated based on thin section analysis
241 (the zones are undifferentiated because the biostratigraphers were not confident in their ability to identify
242 the taxon differentiating the zones, *Parvularugoglobigerina eugubina*, in thin section; Sigurdsson et al.,
243 1997). Shipboard biostratigraphy in the Paleocene is of poor quality due to the extremely poor
244 preservation of fossil material in the indurated limestone. Fortunately, a magnetic polarity timescale was
245 published for Site 1001 by Louvel and Galbrun (2001) based on whole core scans and single samples, as
246 well as a downhole wireline tool called the Geological High-sensitivity Magnetic Tool (GHMT), and the
247 resulting magnetic reversal timescale means that Site 1001 has the best age model of the sites examined
248 here. Although Hole 1001B recovered a more complete boundary section than Hole 1001A (Figure 2B),
249 Hole 1001B has a number of coring gaps in both the uppermost Cretaceous and the early Paleocene, so
250 XRF scans were conducted on Hole 1001A.

251 Site 999 was also drilled in 1995-6 during Leg 165 and is located on a small feature called Kogi
252 Rise in the Colombian Basin (Figure 1). Shipboard biostratigraphy placed the K-Pg boundary near the
253 boundary between Cores 999B-59R and 999B-60R (Figure 2C). The highest occurrence of common
254 Maastrichtian calcareous nannoplankton was observed in Sample 999B-60R-1 10 cm, and that of
255 Maastrichtian planktic foraminifera in a thin section in Sample 999B-60R-1 1-21 cm (Sigurdsson et al.,
256 1997). The few foraminifera observed in thin section between Samples 999B-59R-CC 15cm (the base of
257 the core catcher) and 999B-60R-1 1 cm were composed primarily of survivor species *Guembelitra*
258 *cretacea* (Sigurdsson et al., 1997). The shipboard biostratigraphers were not confident that tiny
259 trochospiral specimens observed in the same sample were or were not *P. eugubina* and thus
260 conservatively assigned this interval to Zones P0/P α undifferentiated (Sigurdsson et al., 1997). The bases
261 of Zones P1a (top of *P. eugubina*), P1b (base of *Subbotina triloculinoides*), and P2 (base of *Praemurica*
262 *uncinata*) were identified shipboard (Sigurdsson et al., 1997) and form the basis for the age model used

263 here, although the latter two are of lower confidence. We washed and examined samples from Site 999 to
264 see if we could refine the shipboard age model but poor microfossil preservation in the indurated
265 limestone material prevented us from adding anything new. A white indurated limestone overlies the
266 highest Cretaceous nannoplankton observed in Core 60, and the base of Section 59R-CC contains a 1 mm
267 thick claystone. Comparison of the recovered core and borehole images collected by the formation
268 microscanner tool reveals that this claystone is ~ 9 cm thick in the borehole, and thus ~ 8 cm of this unit
269 were not recovered (Sigurdsson et al., 1997). It seems reasonable to assume that this missing interval is
270 equivalent to the 8 cm of ejecta-bearing claystones described at Site 1001. The claystone is overlain by
271 10 cm thick mottled blue limestone described by shipboard scientists as having the appearance of
272 “Roquefort Blue Cheese” and assigned to planktic foraminifer Zones P0/P α (Sigurdsson et al., 1997).
273 This white limestone is a common feature of K-Pg boundary sections in the deep sea, and is comprised of
274 micrite (i.e., microcrystalline calcite; Bralower et al., 2020). Although the white limestone only extends
275 10 cm above the boundary, Bralower et al. (2020) observed micrite at Site 999 over a total thickness of
276 2.42 m. A 2 m coring gap occurs at the base of Core 999B-58R in planktic foraminifer Zone P1a. Micrite
277 was also identified at Site 1001 but it was limited to the core catcher of core 1001A-38R, which contains
278 a few discontinuous bits of rubble and a large void space (Figure 2B), so Bralower et al. (2020)
279 considered the observed 17 cm interval to be a minimum.

280 **2. Methods**

281 We scanned the cores at the XRF Core Scanning Lab at the IODP Gulf Coast Repository at Texas
282 A&M University in College Station, TX. The archive halves of selected cores were scraped to ensure a
283 fresh face of the core for scanning, and, in the case of the softer sediments of Site 95, to ensure a flat
284 surface for the XRF core scanner (the split surface was generally smooth in the unlithified cores from Site
285 95 but decades in shrink wrap and added a bit of texture in some places). Lithified sections from Sites 999
286 and 1001 were likewise scraped and leveled within the core liner to ensure a flat horizontal surface. Cores
287 were then covered with 4 μ m thick Ultralene film to prevent sediment from sticking to the scanner.

288 Cores were scanned on an Avaatech XRF Core Scanner at two excitation conditions focused on
289 different element groups. The first scan was at 10kVp with no filter to analyze major and minor elements
290 (Al, Si, K, Ca, Ti, Mn, Fe, Cr, P, S, and Mg) and the second was at 50kVp with a Cu filter to analyze
291 heavier trace elements (Sr, Rb, Zr, and Ba). Scan resolution was set depending on relative distance above
292 the K-Pg boundary, based on low resolution shipboard biostratigraphy. Core sections within Zone P α or
293 the lower part of Zone P1a (very roughly, within ~ 500 kyr after the boundary) were scanned at 1 or 2 cm
294 steps, and sections below the boundary and >500 kyr after the boundary were scanned at 5 cm steps.
295 Some steps were skipped or moved based on visual examination of the core before scanning (e.g., to
296 avoid cracks or uneven surfaces). Laboratory standards were run at the beginning and end of each day to
297 monitor instrumental performance.

298 Raw spectral data were processed into peak areas in the lab using the software program bAxil.
299 Quality control of processed data was carried out using the following parameters: 1) throughput (samples
300 with values <150,000 cps, which indicates a gap between the sensor and the core, were removed); 2)
301 Argon peak (samples with positive Ar values, indicating that the sensor was measuring ambient air, were
302 removed); and 3) standard deviation (samples with elemental peaks of Ba or Ti within 2 standard
303 deviations of zero were removed).

304 To improve the age model for this study we analyzed planktic foraminifera from Site 95 at a
305 resolution of up to 5 cm. Lightly lithified samples were gently broken into cm-sized pieces using a mortar
306 and pestle. All samples were soaked in a solution of hydrogen peroxide and borax for at least 48 hours
307 and then washed over a 45 μ m sieve to ensure capture of typically very small early Paleocene taxa; the
308 sieve was soaked in methylene blue dye between samples to mark contaminants. Finally, samples were
309 dried overnight in an oven. Samples were examined for presence/absence of key marker species on a
310 Zeiss Discovery.V8 light microscope. Species concepts follow those of Olsson et al., (1999); biozones are
311 the Wade et al. (2011) update of the Paleocene biozonation scheme published by Berggren and Pearson
312 (2005) and calibrated to the timescale of Gradstein et al. (2012).

313 3. Results

314 3.1 Biostratigraphy

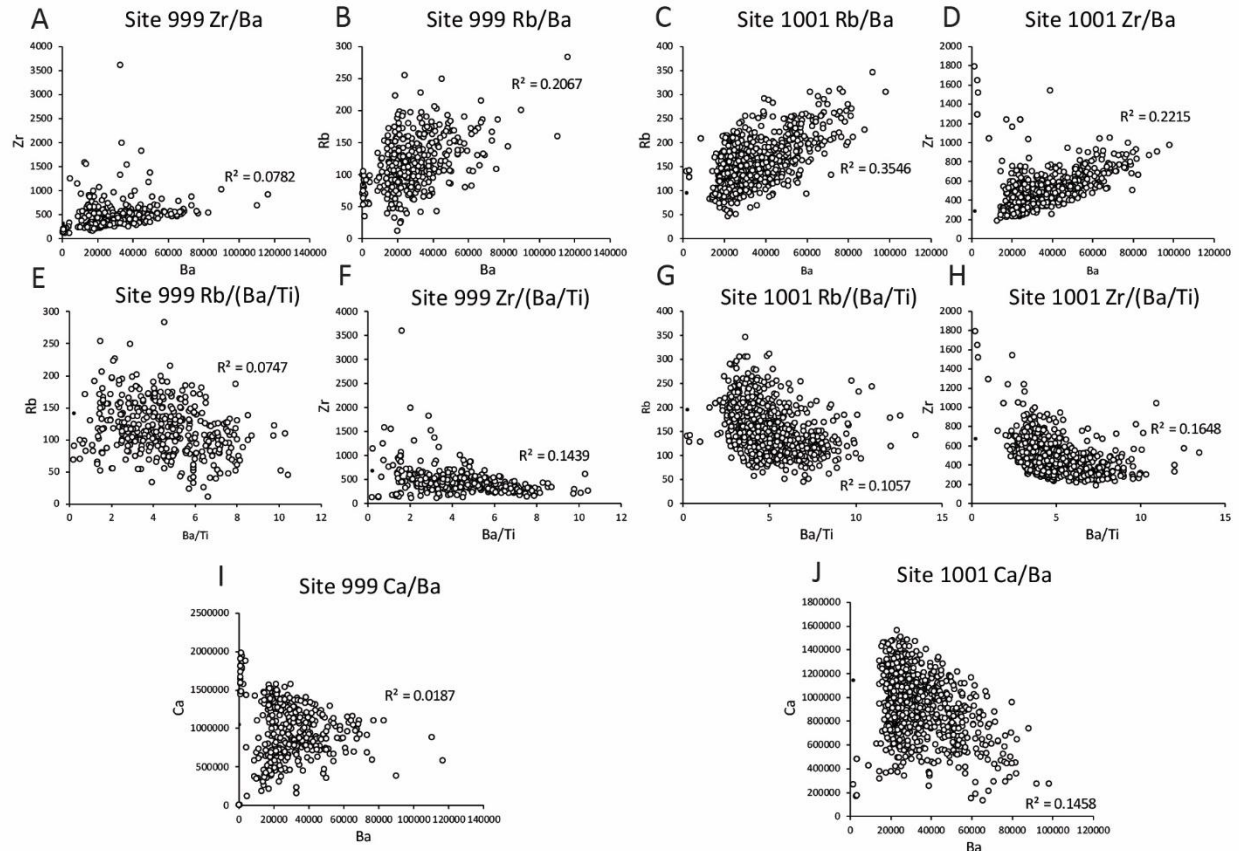
315 Site 95 is comprised of firm but unlithified calcareous ooze that yielded fairly well preserved
316 material. We examined 25 samples from Cores 11 to 13 to identify and then refine the boundaries
317 between planktic foraminifer biozones. An obvious lithologic change occurs in Section 95-13R-3 at 24
318 cm (397.92 mbsf). Samples below this level are composed of mixed Cretaceous species remobilized by
319 impact-induced seismic disturbance and tsunamis, termed the K-Pg Boundary Cocktail (Bralower et al.,
320 1998). From Sample 95-13R-2, 139 cm to Sample 95-13R-3, 24 cm (397.76 to 397.92 mbsf), the core is
321 mottled and contains some signs of drilling disturbance (biscuiting, soft sediment deformation). Samples
322 taken within what we interpret to be the biscuits, however, contain mostly Cretaceous species until 95-
323 13R-3, 0-2 cm (397.70 mbsf), where the survivor species *Guembelitra cretacea* starts to become more
324 common; this level is assigned to the base of Zone P0. The lowest occurrence of *P. eugubina*, which
325 defines the base of Zone P α , is found just above this level, in Sample 95-13R-2 130-132 cm (397.5 mbsf).
326 The highest occurrence of *P. eugubina*, which marks the base of Zone P1a, occurs in sample 95-13R-1
327 130 cm (396.60 mbsf). Most of Zone P1a is erased by a coring gap, but Zone P α and the portion of Zone
328 P1a preserved here contain abundant calcispheres, the resting cyst of calcareous dinoflagellates. Above
329 the coring gap between Cores 95-12R and 13R, the bases of Zone P1b (lowest occurrence of *S.*
330 *triloculinoides*) and Zone P1c (lowest occurrence of *Globanomalina compressa*) are both present. The
331 base of Zone P2 (*P. uncinata*) is missing in another coring gap between Cores 11R and 12R, and the age
332 model from the base of Zone P1c to the coring gap is based on extrapolating the sedimentation rate from
333 Zone P1b; this method suggests that most of Zone P1c is present.

334 3.2 Ba/Ti

335 A key underlying assumption in the use of XRF scan data to reconstruct changes in biogenic Ba
336 is that there is no change in the Ba/Ti ratio of terrigenous material delivered to the site. The extensive

337 volcanism documented in the Caribbean region throughout the early Cenozoic (Sigurdsson et al., 1997)
338 could be a source of discrete or diffuse tephra deposition to the study sites which may vary through time
339 and alter that ratio. Thus, we have plotted Ba from Site 999 and 1001 against Rb and Zr, which are
340 enriched in volcanogenic minerals. Both Zr and Rb show weak positive correlation with Ba at Site 999
341 (Figure 3A-B) and a slightly less-weak positive correlation with Ba at Site 1001 (Figure 3C-D). This is to
342 be expected, as any volcanic ash would have introduced more detrital Ba in the record. However, when
343 we normalize Ba against Ti and compare this to Rb and Zr at both sites, the positive correlation goes
344 away (Figure 3E-H). To demonstrate how overall changes in lithology affect Ba abundance, we plotted
345 Ba against Ca (any decrease in Ca in a pelagic setting above the lysocline is likely due to dilution by
346 terrigenous material). At both sites, there is a weak negative correlation between Ca and Ba (Figure 3I-J).
347 This is what we'd expect, as dilution of pelagic Ca by terrigenous material would introduce detrital Ba;
348 this is also precisely why we normalize Ba to a terrigenous element like Ti, to eliminate any signal from
349 terrigenous Ba. Overall, the relationship between Ca and Ba is not very strong, likely because overall
350 terrigenous content in these pelagic clays is very low. We conclude that the Ba/Ti ratios at these sites do
351 not reflect changes in terrigenous flux from either volcanism or other sources, and are thus primarily
352 driven by changes in export productivity.

353



354

Figure 3. Crossplots of Rb, Zr, and Ca with Ba and Ba/Ti ratios from Sites 999 and 1001. R^2 values showing correlation (or lack thereof) for each parameter are included on the plots.

355 **3.2.1 Site M0077**

356 Data from the Chicxulub Crater have been published previously (Lowery et al., 2018, 2021) but
 357 contain several interesting trends that should be summarized here. The highest Ba/Ti ratios in the study
 358 interval are found in the earliest Paleocene, representing the first ~320 kyr after the impact (Figure 3A).
 359 At that point, there is a sharp drop in Ba/Ti values, followed by a steady decline from moderate values to
 360 a minimum about 1.2 myr after the K-Pg boundary, at which point values stabilize and remain low with
 361 some small-scale variability. Interestingly, this transition around 1.2 myr post-impact coincides with
 362 turnover in the calcareous nannoplankton ecosystem, as disaster taxa began to give way to acmes of new
 363 Paleocene taxa (Jones et al., 2019; Lowery et al., 2021).

364 **3.2.2 Site 95**

365 Ba/Ti ratios at Site 95 are also highest in the earliest Paleocene, with a peak around the P α /P1a
366 zonal boundary and a sharp drop off ~340 kyr after the impact. A difference of 20 kyr between two sites
367 whose age models are entirely based on biostratigraphy is basically within error and we feel comfortable
368 assuming that this drop was contemporaneous with the one observed at Chicxulub Crater Site M0077.
369 Approximately 300 kyr of the record in the middle of Zone P1a is erased by a coring gap, but above this
370 level Ba/Ti values trend lower until about 1.1 myr after the K-Pg boundary. Values then remain low until
371 about 1.6 myr post-impact and finally increase somewhat, varying through the rest of the record.

372 **3.2.3 Site 1001**

373 Site 1001 is the first of our sites in which there are data for the uppermost Cretaceous, and we can
374 see that (above a gap where the boundary layer is mostly missing) Ba/Ti values increase in the Danian
375 relative to the Maastrichtian. Although there is no obvious large peak like in the two Gulf of Mexico sites,
376 there is still an interval of overall higher values lasting to ~ 280 kyr after the impact. Above this level,
377 values are much more variable than in the Gulf of Mexico but there is still a clear downward trend to a
378 nadir around 1.4 myr after the K-Pg boundary, above which point values increase slightly and vary a little
379 bit for the rest of the record.

380 **3.2.4 Site 999**

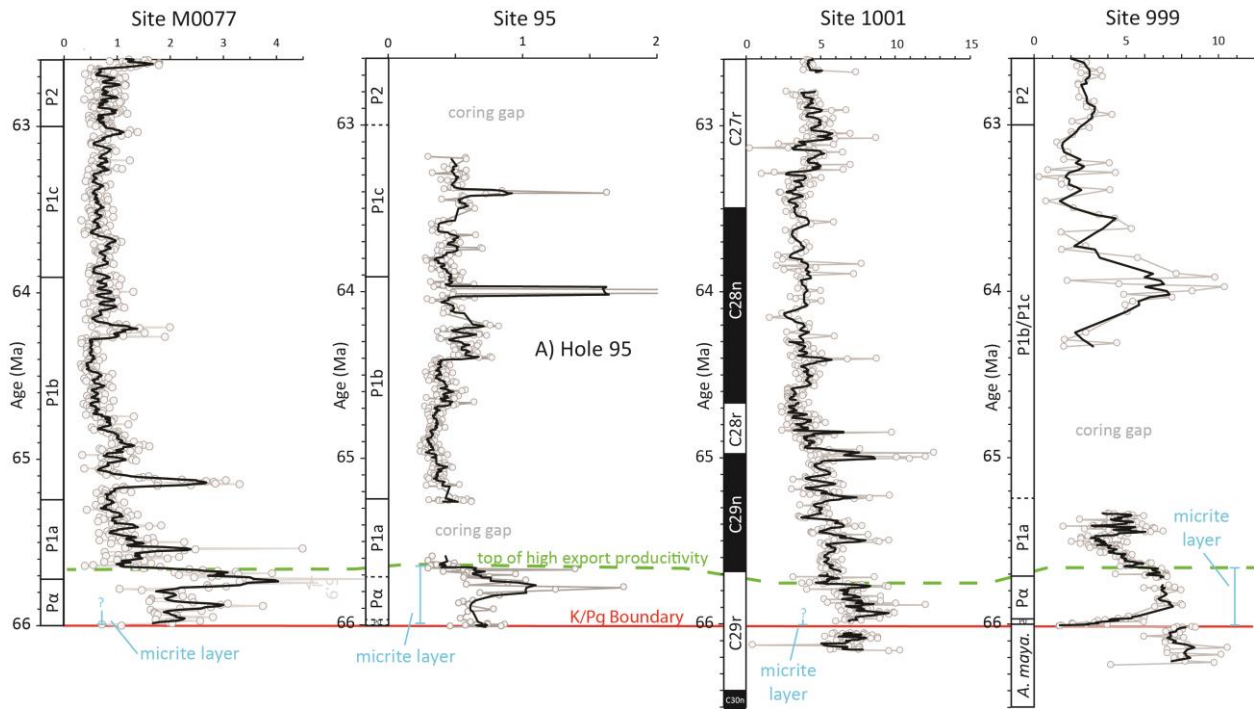


Figure 4. Barium-Titanium export productivity proxy data for IODP Site M0077, DSDP Site 95, and ODP Sites 1001 and 999. Individual datapoints are grey circles, thick black lines is a 5-point moving average. Red line indicates the K-Pg boundary (or the top of the boundary interval in the case of Sites M0077 and 95), blue line indicates the thickness of the micrite layer identified at each site by Bralower et al. (2020), and the green dashed line indicates the top of the interval of highest export productivity at each site. PFZ: Planktic Foraminifer Zone (after Wade et al., 2011); *A. maya.*: *Abathomphalus mayaroensis*.

381 Site 999 is the southernmost site, and the most distal from the Chicxulub impact crater. Ba/Ti
 382 values are very low directly above the boundary layer, quickly increasing through the lower part of Zone
 383 P α . Higher values after this brief recovery interval do not exceed the Ba/Ti values observed in the
 384 uppermost Cretaceous, but they are much higher than subsequent Paleocene values (with the exception of
 385 a brief peak around 2 myr after the K-Pg boundary). Once again, there is a sharp decrease in values
 386 approximately 320 kyr post-impact followed by gradually declining values. The very poor quality of the
 387 biostratigraphy in this core (the P α /P1a zonal boundary marker is really the only reliable datum) makes it
 388 difficult to determine the timing of this decline and whether the increase observed below the coring gap
 389 really occurs just 600 kyr after the boundary or much later. While we do not place much confidence in the
 390 ages above this level, we are confident in age control in the key interval above the boundary, specifically
 391 the highest occurrence of *P. eugubina* (P α /P1a zonal boundary).

392 4. Discussion

393 4.1 Regional Homogeneity of Post K-Pg Export Production

394 The most striking feature of the four export productivity records presented here, and the key
395 result of this investigation, is the consistent occurrence of relatively elevated Ba/Ti values in the earliest
396 Paleocene. Interestingly, this is in line with trends from other sites in oligotrophic regions like the North
397 Pacific Gyre. Three other open ocean sites have evidence of increased export productivity in the earliest
398 Danian: the North Pacific Shatsky Rise and Hess Rise (Alegret and Thomas, 2005, 2009; Hull and Norris,
399 2011), and the mid-latitude South Pacific sections around Marlborough, South Island, New Zealand
400 (Hollis et al., 1995, 2003). The high export productivity at Marlborough appears to be the result of
401 increased upwelling along the continental margin (Hollis et al., 2003). Shatsky Rise and Hess Rise,
402 though, are open ocean sites on roughly the same paleolatitude as our study area and were generally
403 oligotrophic during this time interval (e.g., Deprez et al., 2017; Henehan et al., 2019). It is tempting to
404 interpret the Ba/Ti data as elevated export production in the earliest Paleocene at all of these sites, in
405 contrast with the overall global trend of reduced export production. But first we need to rule out other
406 possible explanations.

407 As discussed above, there is no evidence that changes in terrigenous Ba/Ti ratios influence the
408 record at our Caribbean sites, and in any case this is too regional an explanation to explain how the same
409 trend could be extended to the Gulf of Mexico and North Pacific sites. Likewise, we do not think transient
410 (100-kyr-scale) changes in intermediate or deep water masses affecting barite dissolution rates make
411 sense across such widely dispersed sites. The most likely explanations must be related to the oligotrophic
412 gyres themselves, either oceanographic changes in the gyres themselves or, more likely, ecological
413 changes in the populations of phytoplankton and/or grazers that lived in these gyres.

414 There are several possible mechanisms which could drive an increase in marine barite production
415 while export production is kept steady. Different groups of plankton incorporate different amounts of Ba

416 into their biomass. For example, coccolithophores have less Ba in their cells than diatoms, which in turn
417 have less Ba in their cells than chrysophytes (gold algae), which have less Ba than chlorophytes (green
418 algae) (e.g., Paytan and Griffith, 2007). Calcareous nannoplankton suffered a severe extinction at the K-
419 Pg, and if they were briefly replaced in oligotrophic gyres by any of these other groups, then biogenic Ba
420 flux to the seafloor would increase even if export production held steady. Alternatively (or additionally),
421 an increase in temperature or a shift in bacterial ecology at mesopelagic depths could have increased
422 bacterial remineralization and thus barite production. A reduction in the abundance of grazers which
423 break apart sinking POM or an increase in ballasting or the formation of aggregates (which have the
424 effect of making POM sink more quickly) may have increased the amount of POM which sank below the
425 mesopelagic zone and to the seafloor. However, such a change wouldn't necessarily be expressed by
426 increased biogenic barium, since marine barite formation is a byproduct of the remineralization of organic
427 matter (Dehairs et al., 2008; Jacquet et al., 2011; Planchon et al., 2013) and quickly sinking POM has less
428 time to remineralize. On the other hand, a more robust grazer community at mesopelagic depths may have
429 broken apart more POM, slowed sinking and increased the time it was exposed to remineralization,
430 although it is difficult to imagine a more robust grazer community after a major mass extinction. Many of
431 these change (mesopelagic temperature increase, shifts in the grazer community or toward phytoplankton
432 with higher Ba abundance in their cells) are impossible to test for with existing paleoceanographic tools.
433 What we can do, though, is look to other parts of the biological pump and see if they indicate whether the
434 observed increase in Ba/Ti is indeed related to export productivity.

435 Benthic foraminiferal accumulation rate and assemblages provide additional export productivity
436 information at these sites. Benthic foraminifera, which are responsive to the amount and quality of
437 organic matter that reaches the seafloor, record a different part of the biological pump than biogenic
438 barium, which is formed during the remineralization of organic matter at mesopelagic depths. Indeed,
439 these two proxies can sometimes show opposite trends (e.g., Griffith et al., 2021), which can help us
440 determine if our observations are the result of increased export production or some other process. At Site

441 M0077 in the Chicxulub Crater, elevated Ba/Ti ratios are associated with an interval of higher benthic
442 foraminiferal abundance, indicating increased export production was associated with increased food
443 supply to the seafloor (this was no doubt helped by the fact that the seafloor was at mesopelagic depth;
444 Lowery et al., 2018) (Lowery et al., 2021). Unfortunately, we don't have benthic foraminifera data from
445 Site 95 because it is difficult to tell reworked benthics from *in situ* ones there, and we don't have benthic
446 foraminifera from Sites 999 and 1001 because of overall poor preservation of microfossils. On Shatsky
447 Rise in the North Pacific gyre benthic foraminifera from Site 1210 (from Alegret and Thomas, 2009) and
448 barium proxy data from the adjacent Site 577 (from Hull and Norris, 2011) are elevated for roughly the
449 first 100 kyr after the extinction. On Hess Rise, also in the North Pacific gyre, no barium data exist but
450 benthic foraminifera at Site 465 indicate a peak in post K-Pg burial flux within 100 kyr of the boundary
451 (within planktic foraminifer Zone P α) (Alegret and Thomas, 2005). At the three sites with both Ba and
452 benthic foraminifer data exist, they indicate increased transport of POM out of the euphotic zone and to
453 the seafloor; we therefore interpret the Ba/Ti data at all our sites as primarily recording an increase in
454 export productivity.

455 In the Gulf of Mexico and Caribbean, the interval of highest export production ends right around
456 the P α /P1a zonal boundary at each site, roughly 300 kyr after the K-Pg boundary, followed by a general
457 decline over the next million years or so. The precise features of this record vary from site to site; notably,
458 the prominent early peak observed in the Gulf of Mexico (Sites M0077 and 95) is absent in the Caribbean
459 cores (Sites 999 and 1001). Likewise, Site 999 records very low values immediately above the K-Pg
460 boundary followed by a rapid recovery of values that is not evident at any of the other sites. Finally, the
461 timing of the sharp decline of these high productivity intervals varies by a few tens of kyrs between sites.
462 Because the age models are based on biostratigraphy *or* paleomagnetic reversals, with no higher
463 resolution techniques like orbital chronology, it is impossible to say whether these differences are real or
464 merely artifacts of the limits of the age models. These are superficial differences, though, and a clear

465 overall trend exists that export productivity was elevated across Gulf of Mexico and Caribbean (a distance
466 of ~1700 km) for ~300 kyr after the K-Pg mass extinction, and began to decline thereafter.

467 The observed homogeneity in regional export productivity in the earliest Paleocene provides
468 important context for previous observations of global-scale heterogeneity determined with the Ba proxy.
469 Previous work had shown major differences in the amount of organic matter remineralized in the
470 mesopelagic zone between ocean basins, with an increase in export production observed in the middle of
471 the North Pacific, a decline in the western North Atlantic, western South Atlantic, and Southern Ocean,
472 and no change in the eastern South Atlantic (Hull and Norris, 2011). Those sites are widely separated and
473 represent different oceanographic environments (oligotrophic gyres, western boundary currents, eastern
474 boundary currents). With only one site in each region, it is hard to know whether these observations are
475 indicative of regional trends or more limited, local change. With the discovery that sites within the Gulf
476 of Mexico/Caribbean all exhibit the same trends, we can be more confident that previously observed
477 regional differences are real, and therefore conclude that oligotrophic open ocean sites were prone to
478 increased export production immediately after the K-Pg boundary, as suggested by Henehan et al. (2019).
479 But what was the driver for this increased export production?

480 **4.2 Drivers of Post-Extinction Export Productivity**

481 In the modern ocean, oligotrophic gyres are typically dominated (in terms of biomass) by
482 picophytoplankton (0.2-2.0 μm in size) like cyanobacteria and algae, but larger nano and micro
483 phytoplankton (2-20 μm and $>20 \mu\text{m}$, respectively), though less numerous, account for the majority of
484 productivity measured in incubation experiments (e.g., Marañón et al., 2003). Because picophytoplankton
485 have no fossil record, we cannot say for sure whether this was the case at the end of the Cretaceous, but
486 this seems like a safe assumption.

487 A switch from calcareous nannoplankton, the dominant phytoplankton of the Cretaceous (Bown,
488 2005) to smaller phytoplankton like cyanobacteria and chlorophyte algae would serve to reduce export

489 flux globally and retain more nutrients in the euphotic zone, because smaller cell sizes sink more slowly
490 and are less likely to be consumed by zooplankton and packaged in fecal pellets, or bunch together in
491 aggregates (Legrendre and Michaud, 1998; de la Rocha and Passow, 2007, although it should be noted
492 that some modelling studies dispute the role of plankton size on export, e.g., Fakhraee et al., 2020).
493 Henehan et al. (2019) pointed out that in oligotrophic regions, this post-extinction increase in nutrients
494 could actually lead to an increase in primary and/or export productivity.

495 But how would NPP dominated by picophytoplankton lead to increased export production? After
496 all, if export increased then there would be a mechanism to remove nutrients from the euphotic zone and
497 NPP would necessarily decrease. Yet our work and that of others has found that high export production
498 was maintained in typically oligotrophic regions for 100-300 kyr (Alegret and Thomas, 2005, 2009; Hull
499 and Norris, 2011). To explain this dichotomy, we suggest that POM exported from the euphotic zone
500 became more refractory. The continuous remineralization of very small POM in the euphotic zone is
501 termed the “microbial loop”, and the only POM that manages to sink out of the euphotic zone is more
502 refractory and difficult to metabolize (Legrendre and Michaud, 1998; de la Rocha and Passow, 2007).
503 This refractory organic matter is less likely to be completely remineralized by grazers as it sinks through
504 intermediate depths, which would result in less marine barite formation and lower Ba contents. However,
505 if NPP increased after the K-Pg boundary at these sites as a result of the loss of larger phytoplankton, then
506 the export of refractory POM would also have increased, as would the amount of barite formation from
507 that POM. Thus, even if only a small fraction of the refractory POM was remineralized, the overall
508 increase in POM sinking below the euphotic zone would have elevated total remineralization and barite
509 production. This also would explain why food supply increased to the seafloor, as evidenced by increases
510 in benthic foraminifera.

511 An alternate explanation could be the occurrence of blooms of specific groups of phytoplankton
512 with barium-rich cells or which favor barite formation. For example, in the modern ocean *Phaetocystis* is
513 a common haptophyte which secretes extracellular polymers which form aggregates that speed sinking

514 and enhance export production (e.g., Verity et al., 2007). These polymers may also play a key role in
515 marine barite formation as nucleation sites (Martinez-Ruiz et al., 2020). Acantharians have barium-rich
516 skeletons and are known to form blooms in oligotrophic regions (e.g., Decelle et al., 2012) but, like the
517 other groups, do not typically fossilize. Blooms of plankton like this may serve to increase export to the
518 seafloor and also increase marine barite production without necessarily relying on a stronger microbial
519 loop in the euphotic zone. While we currently lack direct evidence of blooms of non-fossilizing
520 phytoplankton like these groups, more work is required to provide a clear answer to this question. But we
521 can see some evidence for ecosystem changes associated with increased export productivity after the K-
522 Pg.

523 **4.3 Evidence of Ecosystem Changes**

524 The second-most striking feature of our data is that at two of the sites studied (Sites 95 and 999)
525 the interval of high export productivity ~300 kyr after the boundary coincides almost exactly with well-
526 defined intervals of microcrystalline calcite (“micrite”). The widespread deposition of micrite in marine
527 settings after the K-Pg boundary was documented by Bralower et al. (2020), and proposed to be primarily
528 formed by microbial blooms. The structure of individual micrite crystals is similar to that produced by
529 various cyanobacteria (Bralower et al., 2020) and the micrite layer itself at several sites is associated with
530 elevated biomarkers for photosynthetic bacteria and eukaryotic algae (Sepúlveda et al., 2009; Schaefer et
531 al., 2020; Bralower et al., 2020). Some portion of the global micrite layer was also likely formed by the
532 backreaction of CaO or CaOH vaporized by the Chicxulub impact, but this process would have been
533 limited to the years after the impact as ejecta fell out of the atmosphere (Bralower et al., 2020) and
534 wouldn’t explain micrite deposition over ~300 kyr.

535 Extensive recrystallization of carbonate material at Site M0077 obscures the micrite record at that
536 location. At Site M0077, abundant micrite is limited to a zone of good preservation which includes the
537 “Transitional Unit” at the top of the K-Pg boundary layer (Morgan et al., 2017) and an overlying layer of
538 green marlstone dated to the base of planktic foraminifer Zone P α (Bralower et al., 2020). Above this in

539 the overlying white limestone layer, poor preservation prevents the consistent identification of micrite,
540 and so the top of the micrite layer is not identified. At Site 1001, coring gaps in the boundary interval in
541 Hole 1001B limit the identification of the micrite layer to a minimum thickness (17 cm, Bralower et al.,
542 2020). Thus, we have two sites showing a clear deposition of micrite ending at the same stratigraphic
543 position (Sites 95 and 999), and two other sites with insufficient data to determine the relative timing
544 (Sites M0077 and 1001).

545 Unfortunately, none of the previously published Pacific sites which show an increase in post-K-
546 Pg export production have both Ba/Ti data and micrite data (although we can compare nearby sites 1210
547 and 577 – see below). Micrite is enriched at Shatsky Rise Site 1209 over a 6 cm interval above the
548 boundary, and at 1210 over a 7 cm interval above the boundary (Bralower et al., 2020), associated with
549 the ~ 100 kyr peak in benthic foraminifer proxies for burial flux (Alegret and Thomas, 2009) and the ~
550 100 kyr interval of elevated Ba/Ti at nearby Site 577 (Hull and Norris, 2011). At Hess Rise Site 465,
551 micrite is enriched over a 24 cm interval above the boundary (Bralower et al., 2020), and benthic
552 foraminifera likewise show a peak in burial flux in this interval (Alegret and Thomas, 2005). It is
553 important to point out that foraminifer samples at both Sites 465 and 1210 were taken at a 10 cm
554 resolution (Alegret and Thomas, 2005, 2009) so a precise tie between the decline in export productivity
555 and the end of micrite deposition is impossible to make with existing data.

556 Although various types of “ballast,” including calcite plankton shells, have been thought to
557 influence export production in the modern ocean (Amrstrong et al., 2001; Francois et al., 2002), it does
558 not seem likely that micrite itself, or more specifically the cyanobacteria that produced it, is the cause of
559 increased export production in the earliest Paleocene. Micrite is abundant at many sites which did not
560 experience elevated export production after the K-Pg. For example, Blake Nose Site 1049, which
561 experienced either a decline or no change in export production after the boundary (Alegret and Thomas,
562 2007), has a 30 cm thick micrite layer. Walvis Ridge Site 1267, which similarly experienced no change in
563 post-extinction export production based on benthic foraminifera (Alegret and Thomas, 2005), has a 1.82

564 m thick micrite layer. All told, Bralower et al. (2020) identified micrite layers at 31 sites globally; of
565 these, only 5 record elevated export production in the early Danian based on available proxies. All of
566 these sites are in open ocean settings which are predisposed to oligotrophy.

567 The general association of the micrite layer (indicating dominance of microbial primary
568 producers) with the elevated post-impact export production observed across Pacific and Caribbean/Gulf
569 of Mexico sites described here suggests that a post-extinction dominance of picophytoplankton is the
570 primary mechanism driving elevated export productivity at previously oligotrophic parts of the open
571 ocean in the earliest Paleocene.

572 While it appears that the dominance of picophytoplankton is the proximal cause of elevated post
573 K-Pg export production in tropical open ocean waters, it is important to note that the timing is different
574 between the Caribbean and the central Pacific. The period of highest export production drops off ~ 300
575 kyr after the K-Pg in the Gulf of Mexico and Caribbean but ends much earlier at Shatsky and Hess Rises,
576 after ~ 100 kyr (Alegret and Thomas, 2005, 2009; Hull and Norris, 2011). This is in line with previous
577 results which indicate a global diachroneity in the turnover of calcareous nannoplankton assemblages in
578 the earliest Paleocene (Jones et al., 2019), driven by transition from surface waters characterized by
579 efficient recycling of nutrients due to the prevalence of picophytoplankton feeding the microbial loop, to
580 surface waters characterized by less efficient recycling of nutrients caused by greater export of larger
581 plankton out of the euphotic zone (Jones et al., 2019; Lowery et al., 2021). At Shatsky Rise, disaster
582 assemblages of calcareous nannoplankton gave way to acmes of Paleocene taxa soon after the K-Pg
583 (Alvarez et al., 2019; Jones et al., 2019). On the other hand, disaster taxa in the Chicxulub Crater continue
584 until the final decline in export productivity about a million years after the K-Pg (Jones et al., 2019), and
585 at Site 999, disaster taxa continue at least into Zone P1a >300 kyr after the K-Pg (Sigurdsson et al., 1997).
586 Whether the recovery in calcareous nannoplankton caused the observed change in export production or if
587 a reduction in export production spurred the local diversification of calcareous nannoplankton remains an
588 open question.

589 **Conclusions**

590 Our new XRF-derived Ba/Ti export productivity proxy data from the Gulf of Mexico and
591 Caribbean show a post K-Pg peak in export productivity across the region, with an interval of high values
592 lasting for ~ 300 kyr after the boundary and then declining values for another ~ 700 kyr. This is a major
593 improvement on previous compilations of earliest Paleocene export productivity, which showed that post-
594 extinction changes in export production were globally heterogeneous but only on an ocean basin scale.
595 Our results show that broad regions followed similar trends. In particular, we find that most elevated
596 export production in the earliest Danian is found at tropical open ocean sites (Shatsky Rise, Hess Rise,
597 and our Caribbean/Gulf of Mexico sites) which were oligotrophic at the end of the Cretaceous (Henehan
598 et al., 2019).

599 Our other major observation is that at sites with elevated export production and at which
600 preservation makes such observations possible, the post K-Pg global micrite layer corresponds with the
601 interval of elevated export production. We interpret this as evidence that the dominance of
602 picophytoplankton like cyanobacteria and chlorophyte algae, which appear to be associated with the
603 micrite deposition (Bralower et al., 2020), altered the dynamics of the biological pump to increase
604 recycling of organic matter in the euphotic zone. Enhanced recycling of organic matter left only refractory
605 material, which is more difficult to recycle, to be exported from the euphotic zone. Because it is refractory
606 this organic matter would have been more likely to sink through the water column than more labile
607 material exported under normal conditions. In typically oligotrophic environments, this slight increase in
608 efficiency of the biologic pump could have resulted in overall higher export production; as larger
609 phytoplankton recovered and more labile organic matter was exported and grazed, enhanced export
610 production would have subsided.

611 More datasets from a wider range of latitudes and ocean basins are needed to build a more
612 complete picture of post K-Pg export production to more fully understand how the marine biosphere
613 recovered from the most recent major mass extinction.

614 **Data Availability Statement**

615 XRF core scan data and age models are archived at the NCEI Paleoclimate Database here:

616 <https://www.ncei.noaa.gov/access/paleo-search/study/35081>

617

618 **Acknowledgements**

619 We are grateful for insightful reviews by Ellen Thomas and an anonymous reviewer, both of which
620 substantially improved this manuscript. We are also grateful to Brian LeVay and Mackenzie Schoemann
621 of the IODP Gulf Coast Repository (GCR) at Texas A&M University for their assistance with XRF core
622 scanning, the staff of the GCR for sending samples from Sites 95 and 536 for biostratigraphic analysis,
623 and Vinny Percuoco at the GCR for providing high resolution photograph for the K-Pg boundary in Hole
624 1001B. We are also grateful to Ryan Weber and Calvin Gordon of PaleoData, Inc., for their assistance
625 preparing samples from Site 999 and 1001 for biostratigraphic analysis.

626 **Figure 1.** A) Global plate tectonic reconstruction from 66 Ma showing location of our study area (in red)
627 and other notable sites discussed in this paper (in orange). Grey areas are continental blocks, terranes, and
628 plateaus; map from ODSN generated at <https://www.odsn.de/odsn/services/paleomap/paleomap.html>. B)
629 Regional map showing position of our study sites around the time of the K-Pg Boundary. Map modified
630 after Pindell and Barrett (1990) and Snedden et al. (2021). Black indicates land and grey indicates
631 shelves.

632 **Figure 2.** Stratigraphic sections showing lithostratigraphy, core scan photographs, and images of the K-
633 Pg boundary of the studied intervals from DSDP Hole 95, ODP Hole 1001A, and ODP Hole 999B.
634 Lithostratigraphy follows shipboard descriptions Worzel, Bryant et al. (1973) for Site 95 and Sigurdsson
635 et al., 1997 for Sites 999 and 1001). Core scan photographs were collected at the GCR at the same time
636 XRF data were collected (except for the photograph of the K-Pg boundary in Hole 1001B, which is from
637 the ODP photo archives). Mbsf = meters below sea floor, PFZ = Planktic Foraminifer Zone, Lith. =

638 lithology, PMag = Paleomagnetic polarity, E. Campanian = Early Campanian, Maas. = Maastrichtian, *G.*
639 *elevata* = *Globoetruncanita elevata*, *A.m.* and *A. mayaroensis* = *Abathomphalus mayaroensis*.

640 **Figure 3.** Crossplots of Rb, Zr, and Ca with Ba and Ba/Ti ratios from Sites 999 and 1001. R² values
641 showing correlation (or lack thereof) for each parameter are included on the plots.

642

643 **Figure 4.** Barium/Titanium export productivity proxy data for IODP Site M0077, DSDP Site 95, and
644 ODP Sites 1001 and 999. Individual datapoints are grey circles, thick black lines are a 5-point moving
645 average. Red line indicates the K-Pg boundary (or the top of the boundary interval in the case of Sites
646 M0077 and 95), blue line indicates the thickness of the micrite layer identified at each site by Bralower et
647 al. (2020), and the green dashed line indicates the top of the interval of highest export productivity at each
648 site. PFZ = Planktic Foraminifer Zone, *A. maya.* = *Abathomphalus mayaroensis*.

649 **References**

650 Alegret, L., & Thomas, E. (2005). Cretaceous/Paleogene boundary bathyal paleo-environments in the
651 central North Pacific (DSDP Site 465), the Northwestern Atlantic (ODP Site 1049), the Gulf of
652 Mexico and the Tethys: The benthic foraminiferal record. *Palaeogeography, Palaeoclimatology,*
653 *Palaeoecology*, 224(1-3), 53-82.

654 Alegret, L., & Thomas, E. (2007). Deep-sea environments across the Cretaceous/Paleogene boundary in
655 the eastern South Atlantic Ocean (ODP leg 208, Walvis Ridge). *Marine Micropaleontology*, 64(1-
656 2), 1-17.

657 Alegret, L., & Thomas, E. (2009). Food supply to the seafloor in the Pacific Ocean after the
658 Cretaceous/Paleogene boundary event. *Marine Micropaleontology*, 73(1-2), 105-116.

659 Alegret, L., Thomas, E., & Lohmann, K. C. (2012). End-Cretaceous marine mass extinction not caused by
660 productivity collapse. *Proceedings of the National Academy of Sciences*, 109(3), 728-732.

661 Alegret, L., Arreguín-Rodríguez, G. J., Trasviña-Moreno, C. A., & Thomas, E. (2021). Turnover and
662 stability in the deep sea: Benthic foraminifera as tracers of Paleogene global change. *Global and*
663 *Planetary Change*, 196, 103372.

664 Armstrong, R. A., Lee, C., Hedges, J. I., Honjo, S., & Wakeham, S. G. (2001). A new, mechanistic model
665 for organic carbon fluxes in the ocean based on the quantitative association of POC with ballast
666 minerals. *Deep Sea Research Part II: Topical Studies in Oceanography*, 49(1-3), 219-236.

667 Artemieva, N., Morgan, J., & Expedition 364 Science Party. (2017). Quantifying the release of climate-
668 active gases by large meteorite impacts with a case study of Chicxulub. *Geophysical Research*
669 *Letters*, 44(20), 10-180.

670 Artemieva, N., & Morgan, J. (2020). Global K-Pg layer deposited from a dust cloud. *Geophysical*
671 *Research Letters*, 47(6), e2019GL086562.

672 Bains, S., Norris, R. D., Corfield, R. M., & Faul, K. L. (2000). Termination of global warmth at the
673 Palaeocene/Eocene boundary through productivity feedback. *Nature*, 407(6801), 171-174.

674 Bardeen, C. G., Garcia, R. R., Toon, O. B., & Conley, A. J. (2017). On transient climate change at the
675 Cretaceous– Paleogene boundary due to atmospheric soot injections. *Proceedings of the National*
676 *Academy of Sciences*, 114(36), E7415-E7424.

677 Barton, A. D., Irwin, A. J., Finkel, Z. V., & Stock, C. A. (2016). Anthropogenic climate change drives
678 shift and shuffle in North Atlantic phytoplankton communities. *Proceedings of the National*
679 *Academy of Sciences*, 113(11), 2964-2969.

680 Berggren, W. A., & Pearson, P. N. (2005). A revised tropical to subtropical Paleogene planktonic
681 foraminiferal zonation. *The Journal of Foraminiferal Research*, 35(4), 279-298.

682 Birch, H. S., Coxall, H. K., Pearson, P. N., Kroon, D., & Schmidt, D. N. (2016). Partial collapse of the
683 marine carbon pump after the Cretaceous-Paleogene boundary. *Geology*, 44(4), 287-290.

684 Birch, H., Schmidt, D. N., Coxall, H. K., Kroon, D., & Ridgwell, A. (2021). Ecosystem function after the
685 K/Pg extinction: decoupling of marine carbon pump and diversity. *Proceedings of the Royal*
686 *Society B*, 288(1953), 20210863.

687 Bown, P. (2005). Selective calcareous nannoplankton survivorship at the Cretaceous-Tertiary boundary.
688 *Geology*, 33(8), 653-656.

689 Boyd, P. W., & Trull, T. W. (2007). Understanding the export of biogenic particles in oceanic waters: Is
690 there consensus?. *Progress in Oceanography*, 72(4), 276-312.

691 Bralower, T. J., Paull, C. K., & Mark Leckie, R. (1998). The Cretaceous-Tertiary boundary cocktail:
692 Chicxulub impact triggers margin collapse and extensive sediment gravity flows. *Geology*, 26(4),
693 331-334.

694 Bralower, T. J., Cosmidis, J., Heaney, P. J., Kump, L. R., Morgan, J. V., Harper, D. T., ... & Vajda, V.
695 (2020). Origin of a global carbonate layer deposited in the aftermath of the Cretaceous-Paleogene
696 boundary impact. *Earth and Planetary Science Letters*, 548, 116476.

697 Buesseler, K. O., & Boyd, P. W. (2009). Shedding light on processes that control particle export and flux
698 attenuation in the twilight zone of the open ocean. *Limnology and Oceanography*, 54(4), 1210-
699 1232.

700 Buffler, R.T., Schlager, W., et al. (1984). Initial Reports of the Deep Sea Drilling Project 77,
701 doi:10.2973/dsdp.proc.77.1984

702 Coxall, H. K., D'Hondt, S., & Zachos, J. C. (2006). Pelagic evolution and environmental recovery after
703 the Cretaceous-Paleogene mass extinction. *Geology*, 34(4), 297-300.

704 Culver, S. J. (2003). Benthic foraminifera across the Cretaceous-Tertiary (K-T) boundary: a review.
705 *Marine Micropaleontology*, 47(3-4), 177-226.

706 D'Hondt, S., Donaghay, P., Zachos, J. C., Luttenberg, D., & Lindinger, M. (1998). Organic carbon fluxes
707 and ecological recovery from the Cretaceous-Tertiary mass extinction. *Science*, 282(5387), 276-
708 279.

709 De La Rocha, C. L., & Passow, U. (2007). Factors influencing the sinking of POC and the efficiency of
710 the biological carbon pump. *Deep Res II* 54: 639–658.

711 Dehairs, F., Jacquet, S., Savoye, N., Van Mooy, B. A., Buesseler, K. O., Bishop, J. K. B., Lamborg, C.
712 H., Elskens, M., Baeyens, W., Bowd, P. W., Cascotti, K.L., & Monnin, C. (2008). Barium in
713 twilight zone suspended matter as a potential proxy for particulate organic carbon
714 remineralization: Results for the North Pacific. *Deep Sea Research Part II: Topical Studies in*
715 *Oceanography*, 55(14-15), 1673-1683.

716 Deprez, A., Jehle, S., Bornemann, A., & Speijer, R. P. (2017). Pronounced biotic and environmental
717 change across the latest Danian warming event (LDE) at Shatsky Rise, Pacific Ocean (ODP Site
718 1210). *Marine Micropaleontology*, 137, 31-45.

719 Denne, R. A., Scott, E. D., Eickhoff, D. P., Kaiser, J. S., Hill, R. J., & Spaw, J. M. (2013). Massive
720 Cretaceous-Paleogene boundary deposit, deep-water Gulf of Mexico: New evidence for
721 widespread Chicxulub-induced slope failure. *Geology*, 41(9), 983-986.

722 Doyle, P. S., & Riedel, W. R. (1979). Ichthyoliths: present status of taxonomy and stratigraphy of
723 microscopic fish skeletal debris. Scripps Institution of Oceanography, University of California at
724 San Diego.

725 Dymond, J., Suess, E., & Lyle, M. (1992). Barium in deep-sea sediment: A geochemical proxy for
726 paleoproductivity. *Paleoceanography*, 7(2), 163-181.

727 Eagle, M., Paytan, A., Arrigo, K. R., van Dijken, G., & Murray, R. W. (2003). A comparison between
728 excess barium and barite as indicators of carbon export. *Paleoceanography*, 18(1).

729 Esmeray-Senlet, S., Wright, J. D., Olsson, R. K., Miller, K. G., Browning, J. V., & Quan, T. M. (2015).
730 Evidence for reduced export productivity following the Cretaceous/Paleogene mass extinction.
731 *Paleoceanography*, 30(6), 718-738.

732 Fakhraee, M., Planavsky, N. J., & Reinhard, C. T. (2020). The role of environmental factors in the long-
733 term evolution of the marine biological pump. *Nature Geoscience*, 13(12), 812-816.

734 Fraass, A. J., Kelly, D. C., & Peters, S. E. (2015). Macroevolutionary history of the planktic foraminifera.
735 *Annual Review of Earth and Planetary Sciences*, 43, 139-166.

736 Francois, R., Honjo, S., Manganini, S. J., & Ravizza, G. E. (1995). Biogenic barium fluxes to the deep
737 sea: Implications for paleoproductivity reconstruction. *Global Biogeochemical Cycles*, 9(2), 289-
738 303.

739 Francois, R., Honjo, S., Krishfield, R., & Manganini, S. (2002). Factors controlling the flux of organic
740 carbon to the bathypelagic zone of the ocean. *Global Biogeochemical Cycles*, 16(4), 34-1.

741 Gibbs, S. J., Bown, P. R., Ward, B. A., Alvarez, S. A., Kim, H., Archontikis, O. A., Sauterey, B. Poulton, A.
742 J., Wilson, J., & Ridgwell, A. (2020). Algal plankton turn to hunting to survive and recover from
743 end-Cretaceous impact darkness. *Science advances*, 6(44), eabc9123.

744 Gradstein, F. M., Ogg, J. G., Schmitz, M. D., & Ogg, G. M. (Eds.). (2012). *The geologic time scale 2012*.
745 elsevier.

746 Griffith, E. M., & Paytan, A. (2012). Barite in the ocean—occurrence, geochemistry and
747 palaeoceanographic applications. *Sedimentology*, 59(6), 1817-1835.

748 Hallock, P. (1987). Fluctuations in the trophic resource continuum: a factor in global diversity cycles?.
749 *Paleoceanography*, 2(5), 457-471.

750 Henehan, M. J., Ridgwell, A., Thomas, E., Zhang, S., Alegret, L., Schmidt, D. N., Rae, J. W. B., Witts, J.
751 D., Landman, N. H., Greene, S. E., & Hull, P. M. (2019). Rapid ocean acidification and

752 protracted Earth system recovery followed the end-Cretaceous Chicxulub impact. Proceedings of
753 the National Academy of Sciences, 116(45), 22500-22504.

754 Henson, S. A., Sanders, R., & Madsen, E. (2012). Global patterns in efficiency of particulate organic
755 carbon export and transfer to the deep ocean. *Global Biogeochemical Cycles*, 26(1).

756 Hollis, C. J., Rodgers, K. A., & Parker, R. J. (1995). Siliceous plankton bloom in the earliest Tertiary of
757 Marlborough, New Zealand. *Geology*, 23(9), 835-838.

758 Hollis, C. J., Strong, C. P., Rodgers, K. A., & Rogers, K. M. (2003). Paleoenvironmental changes across
759 the Cretaceous/Tertiary boundary at Flaxbourne River and Woodside Creek, eastern
760 Marlborough, New Zealand. *New Zealand Journal of Geology and Geophysics*, 46(2), 177-197.

761 Hsü, K. J., & Mckenzie, J. A. (1985). A “Strangelove” ocean in the earliest Tertiary. *The Carbon Cycle
762 and Atmospheric CO₂: Natural Variations Archean to Present*, 32, 487-492.

763 Hull, P. M., & Norris, R. D. (2011). Diverse patterns of ocean export productivity change across the
764 Cretaceous-Paleogene boundary: New insights from biogenic barium. *Paleoceanography*, 26(3).

765 Jacquet, S. H., Dehairs, F., Dumont, I., Becquevort, S., Cavagna, A. J., & Cardinal, D. (2011). Twilight
766 zone organic carbon remineralization in the Polar Front Zone and Subantarctic Zone south of
767 Tasmania. *Deep Sea Research Part II: Topical Studies in Oceanography*, 58(21-22), 2222-2234.

768 Jiang, S., Bralower, T. J., Patzkowsky, M. E., Kump, L. R., & Schueth, J. D. (2010). Geographic controls
769 on nanoplankton extinction across the Cretaceous/Palaeogene boundary. *Nature Geoscience*,
770 3(4), 280-285.

771 Jones, H. L., Lowery, C. M., & Bralower, T. J. (2019). Delayed calcareous nanoplankton boom-bust
772 successions in the earliest Paleocene Chicxulub (Mexico) impact crater. *Geology*, 47(8), 753-756.

773 Thierstein, H. R. (1982). Terminal Cretaceous plankton extinctions: A critical assessment. *Geological
774 implications of impacts of large asteroids and comets on the earth*, 190, 385-399.

775 Legendre, L., & Michaud, J. (1998). Flux of biogenic carbon in oceans: size-dependent regulation by
776 pelagic food webs. *Marine Ecology Progress Series*, 164, 1-11.

777 Louvel, V., & Galbrun, B. (2000). Magnetic polarity sequences from downhole measurements in ODP
778 holes 998B and 1001A, leg 165, Caribbean Sea. *Marine Geophysical Researches*, 21(6), 561-577.

779 Lowery, C. M., Bralower, T. J., Owens, J. D., Rodríguez-Tovar, F. J., Jones, H., Smit, J., Whalen, M. T.,
780 Claeys, P., Farley, K., Gulick, S. P. S., Morgan, J. V., Green, S., Chenot, E., Christeson, G. L.,
781 Cockell, C. S. Coolen, M. J. L., Ferrière, L., Gebhardt, C., Goto, K., Kring, D. A., Lofi, J.,
782 Ocampo-Torres, R., Perez-Cruz, L., Pickersgill, A. E., Poelchau, M. H., Rae, A. S. P., Rasmussen
783 C., Rebolledo-Vieyra, M., Riller, U., Sato, H., Tikoo, S. M., Tomioka, N., Urrutia-Fucugauchi, J.,
784 Vellekoop, J., Wittmann, A., Xiao, L., Yamaguchi, K. E., & Zylberman, W. (2018). Rapid
785 recovery of life at ground zero of the end-Cretaceous mass extinction. *Nature*, 558(7709), 288-
786 291.

787 Lowery, C. M., Bown, P. R., Fraass, A. J., & Hull, P. M. (2020). Ecological response of plankton to
788 environmental change: thresholds for extinction. *Annual Review of Earth and Planetary Sciences*,
789 48, 403-429.

790 Lowery, C. M., Jones, H., Bralower, T. J., Perez Cruz, L., Gebhardt, C., Whalen, M. T., Chenot, E., Smit,
791 J., Purkey Phillips, M., Choumiline, K., Arenillas, I., Arz, J. A., Garcia, F., Ferrand, M., Gulick,
792 S. P. S., and IODP Expedition 364 Scientists. (2021) Early Paleocene paleoceanography and
793 export productivity in the Chicxulub crater. *Paleoceanography & Paleoclimatology*.

794 Marañón, E., Behrenfeld, M. J., González, N., Mouriño, B., & Zubkov, M. V. (2003). High variability of
795 primary production in oligotrophic waters of the Atlantic Ocean: uncoupling from phytoplankton
796 biomass and size structure. *Marine Ecology Progress Series*, 257, 1-11.

797 Martinez-Ruiz, F., Paytan, A., Gonzalez-Muñoz, M. T., Jroundi, F., Abad, M. D. M., Lam, P. J., Horner,
798 T. J., & Kastner, M. (2020). Barite precipitation on suspended organic matter in the mesopelagic
799 zone. *Frontiers in Earth Science*, 8, 567714.

800 Molina, E., Alegret, L., Arenillas, I., Arz, J. A., Gallala, N., Hardenbol, J., von Salis, K., Steurbaut, E.,
801 Vandenberghe, N., & Zaghbib-Turki, D. (2006). The global boundary stratotype section and point
802 for the base of the Danian stage (Paleocene, Paleogene, "Tertiary", Cenozoic) at El Kef, Tunisia-
803 original definition and revision. *Episodes*, 29(4), 263.

804 Morgan, J., Gulick, S., Mellett, C. L., & Green, S. L. (2017). Chicxulub: drilling the K-Pg impact crater.
805 Proceedings of the International Ocean Discovery Program, 364.
806 <https://doi.org/10.14379/iodp.proc.364.2017>

807 Müller, P. J. and Suess, E., 1979. Productivity, sedimentation rate, and sedimentary organic matter in the
808 oceans—I. Organic carbon preservation. *Deep Sea Research Part A. Oceanographic Research*
809 *Papers*, 26(12), pp.1347-1362.

810 Olsson, R. K., Berggren, W. A., Hemleben, C., & Huber, B. T. (1999). Atlas of Paleocene planktonic
811 foraminifera. *Smithsonian Contributions to Paleobiology* 85, 1-106

812 Passow, U., & Carlson, C. A. (2012). The biological pump in a high CO₂ world. *Marine Ecology*
813 *Progress Series*, 470, 249–272. <http://www.jstor.org/stable/24876215>

814 Paytan, A., Kastner, M., & Chavez, F. P. (1996). Glacial to interglacial fluctuations in productivity in the
815 equatorial Pacific as indicated by marine barite. *Science*, 274(5291), 1355-1357.

816 Paytan, A., & Griffith, E. M. (2007). Marine barite: Recorder of variations in ocean export productivity.
817 *Deep Sea Research Part II: Topical Studies in Oceanography*, 54(5-7), 687-705.

818 Pindell, J. L., & Barrett, S. F. (1990). Caribbean plate tectonic history. *The Caribbean Region, volume H*
819 *of The Geology of North America*, 405-432.

820 Planchon, F., Cavagna, A. J., Cardinal, D., André, L., & Dehairs, F. (2013). Late summer particulate
821 organic carbon export and twilight zone remineralisation in the Atlantic sector of the Southern
822 Ocean. *Biogeosciences*, 10(2), 803-820.

823 Sanford, J. C., Snedden, J. W., & Gulick, S. P. (2016). The Cretaceous-Paleogene boundary deposit in the
824 Gulf of Mexico: Large-scale oceanic basin response to the Chicxulub impact. *Journal of*
825 *Geophysical Research: Solid Earth*, 121(3), 1240-1261.

826 Schaefer, B., Grice, K., Coolen, M. J., Summons, R. E., Cui, X., Bauersachs, T., Böttcher, M.E.,
827 Bralower, T.J., Lyons, S.L. and Freeman, K.H, Cockell, C. S., Gulick, S. P. S., Morgan, J. V.,
828 Whalen, M. T., Lowery, C. M., & Vajda, V. (2020). Microbial life in the nascent Chicxulub
829 crater. *Geology*, 48(4), 328-332.

830 Schueth, J. D., Bralower, T. J., Jiang, S., & Patzkowsky, M. E. (2015). The role of regional survivor
831 incumbency in the evolutionary recovery of calcareous nannoplankton from the
832 Cretaceous/Paleogene (K/Pg) mass extinction. *Paleobiology*, 41(4), 661-679.

833 Sepúlveda, J., Wendler, J. E., Summons, R. E., & Hinrichs, K. U. (2009). Rapid resurgence of marine
834 productivity after the Cretaceous-Paleogene mass extinction. *Science*, 326(5949), 129-132.

835 Sepúlveda, J., Alegret, L., Thomas, E., Haddad, E., Cao, C., & Summons, R. E. (2019). Stable isotope
836 constraints on marine productivity across the Cretaceous-Paleogene mass extinction.
837 *Paleoceanography and Paleoclimatology*, 34(7), 1195-1217.

838 Sibert, E. C., & Norris, R. D. (2015). New Age of Fishes initiated by the Cretaceous– Paleogene mass
839 extinction. *Proceedings of the National Academy of Sciences*, 112(28), 8537-8542.

840 Sigurdsson, H., Leckie, R.M., Acton, G.D., et al., 1997. *Proceedings of the Ocean Drilling Program,*
841 *Initial Reports.*, 165: College Station, TX (Ocean Drilling Program).
842 doi:10.2973/odp.proc.ir.165.1997

843 Snedden, J., Leshyk, V. O., and Kring, D. (2021). Paleogeographic Evolution of the Chicxulub Region.
844 Lunar and Planetary Institute illustration,
845 <https://www.lpi.usra.edu/exploration/training/illustrations/chicxulub-effects/>, accessed 9/27/21.

846 Thierstein, H. R. (1982). Terminal Cretaceous plankton extinctions: A critical assessment. Geological
847 implications of impacts of large asteroids and comets on the earth, 190, 385-399.

848 Toon, O. B., Zahnle, K., Morrison, D., Turco, R. P., & Covey, C. (1997). Environmental perturbations
849 caused by the impacts of asteroids and comets. *Reviews of Geophysics*, 35(1), 41-78.

850 Verity, P. G., Brussaard, C. P., Nejstgaard, J. C., van Leeuwe, M. A., Lancelot, C., & Medlin, L. K.
851 (2007). Current understanding of Phaeocystis ecology and biogeochemistry, and perspectives for
852 future research. *Biogeochemistry*, 83(1), 311-330.

853 Wade, B. S., Pearson, P. N., Berggren, W. A., & Pälike, H. (2011). Review and revision of Cenozoic
854 tropical planktonic foraminiferal biostratigraphy and calibration to the geomagnetic polarity and
855 astronomical time scale. *Earth-Science Reviews*, 104(1-3), 111-142.

856 Worzel, J. L., Bryant, W., et al, 1973, Initial Reports of the Deep Sea Drilling Project, Volume X,
857 Washington (U.S. Government Printing Office) doi:10.2973/dsdp.proc.10.1973

858 Zachos, J. C., & Arthur, M. A. (1986). Paleooceanography of the Cretaceous/Tertiary boundary event:
859 inferences from stable isotopic and other data. *Paleoceanography*, 1(1), 5-26.

860 Zachos, J. C., Arthur, M. A., & Dean, W. E. (1989). Geochemical evidence for suppression of pelagic
861 marine productivity at the Cretaceous/Tertiary boundary. *Nature*, 337(6202), 61-64.

862 Zhang, C., Dang, H., Azam, F., Benner, R., Legendre, L., Passow, U., Polimene, L., Robinson, C., Suttle,
863 C. A., & Jiao, N. (2018). Evolving paradigms in biological carbon cycling in the ocean. *National*
864 *Science Review*, 5(4), 481-499.